J Geod (2014) 88:145–155
DOI 10.1007/s00190-013-0675-7

ORIGINAL PAPER

Long-term polar motion prediction using normal time–frequency transform

Xiaoqing Su · Lintao Liu · Hsu Houtse · Guocheng Wang

Received: 28 May 2013 / Accepted: 24 October 2013 / Published online: 30 November 2013

Abstract This paper presents normal time–frequency transform (NTFT) application in harmonic/quasi-harmonic signal prediction. Particularly, we use the normal wavelet transform (a special NTFT) to make long-term polar motion prediction. Instantaneous frequency, phase and amplitude of Chandler wobble, prograde and retrograde annual wobbles of Earth's polar motion are analyzed via the NTFT. Results show that the three main wobbles can be treated as quasi-harmonic processes. Current instantaneous harmonic information of the three wobbles can be acquired by the NTFT that has a kernel function constructed with a normal half-window function. Based on this information, we make the polar motion predictions with lead times of 1 year and 5 years. Results show that our prediction skills are very good with long lead time. An abnormality in the predictions occurs during the second half of 2005 and first half of 2006. Finally, we provide the future (starting from 2013) polar motion predictions with 1- and 5-year leads. These predictions will be used to verify the effectiveness of the method proposed in this paper.

Keywords Normal time–frequency transform · Harmonic information · Normal window function · Polar motion prediction

X. Su · L. Liu (✉) · H. Houtse · G. Wang
State Key Laboratory of Geodesy and Earth's Dynamics, Institute of Geodesy and Geophysics, CAS, Wuhan 430077, China
e-mail: llt@asch.whigg.ac.cn

X. Su · G. Wang
University of Chinese Academy of Sciences, Beijing 100049, China

1 Introduction

Polar motion is Earth's rotation axis movement with respect to its crust. It is a significant component of Earth orientation parameters (EOPs). In general, EOPs are available with a delay of hours to days because of complex data processing procedures. The growing demand from spacecraft tracking and navigation has intensified the researches on EOP predictions (Kalarus et al. 2010; Xu et al. 2012).

Various techniques have also been developed and applied to the polar motion prediction, including those presented by Petrov et al. (1995), Kosek et al. (1998), Kosek (2002), Schuh et al. (2002), Akulenko et al. (2002), Akyilmaz and Kutterer (2004), Akyilmaz et al. (2011), and Liao et al. (2012). These methods either estimate the parameters of harmonic functions and extrapolate them into the future or use stochastic models such as autoregressive integrated moving average processes and Kalman filter with atmospheric angular momentum forecast. A combination of these methods is used for the polar motion prediction (Xu et al. 2012) and the comparison between these methods has also been conducted (Kalarus et al. 2010; Kosek et al. 2007).

These methods work well for short-term prediction. However, their performance is not satisfactory in mid-term and long-term predictions because of increasing prediction error with lead time. On one hand, the limited prediction accuracy is caused by the variable amplitude of Chandler and annual wobbles and short-period oscillations (which have amplitudes up to several mass and even tens of them) (Zhu 1982). On the other hand, in these methods, the instantaneous harmonic information (including frequency, amplitude and phase) of the polar motion is not taken into account although such information is necessary for the polar motion prediction.

The polar motion is the sum of two statically independent parts: trend and undulation. Thus, polar motion

prediction consists of trend prediction and undulation prediction. A trend item can be obtained via linear least squares adjustment. The acquired fitting parameter can be applied to trend prediction as well.

However, no tool as simple as the linear least squares adjustment exists for undulation prediction which is the focus of this study. The instantaneous frequency, phase and amplitude of the undulation can be obtained via time–frequency analysis. Normal time–frequency transform (NTFT) proposed by Liu and Hsu (2009, 2012) is designed for unbiased measurement of the instantaneous frequency, phase and amplitude of a time series. Its rescaling index $\mu(\varpi)$ can be a constant as in Gabor transform or linear as in wavelet transform, but even quadratic, cubic or any other function can be used to construct other unnamed transforms. The NTFT is used to construct the prediction model that considers the information coming from both time and frequency domains rather than the information coming from pure time or frequency domain. For the first time, this study uses the time–frequency analysis method (i.e., the NTFT) to predict the polar motion.

In practice, the closer to the current time the time series data are, the more useful they are for prediction. However, the edge effect existing in the time–frequency analysis method makes the time–frequency analysis results at the current time (i.e., the end of the observation) implausible. In order to obtain the instantaneous frequency, amplitude and phase at the current time, half-window can be used to construct the kernel function of the NTFT.

This paper is organized as follows. Section 2 introduces the NTFT concept and explains how it works for time–frequency analysis and prediction. In Sect. 3, based on the normal wavelet transform (a special NTFT), we present the time–frequency analysis of the polar motion and illuminate the predictability of long-term polar motion. In Sect. 4, the NTFT with its kernel function using the half-window is applied to the long-term polar motion predictions. Section 5 provides the conclusion.

2 Normal time–frequency transform for prediction

The NTFT has been proposed by Liu and Hsu (2009, 2012); refer to these studies for detailed proof and properties of the NTFT) and is defined as follows.

Definition 2.1 A local time function $w(t) \in L^1(R)$ is called a normal window if

$$\hat{w}(\omega) = \left|\hat{w}(\omega)\right| = \textbf{Maximum} = 1 \Leftrightarrow \omega = 0 \tag{1}$$

where $\hat{w}(\omega) = \mathrm{F}[w(t)]_\omega$, $\mathrm{F}[\cdot]_\omega$ is Fourier transform (FT) operator, "$|\cdot|$" denotes modulus operator, and "$\Leftrightarrow$" means "if and only if". $\hat{w}(\omega)$is a function of ω. Equation (1) means that if and only if $\omega = 0$, function $\hat{w}(\omega) = \left|\hat{w}(\omega)\right|$ and meanwhile $|\hat{w}(\omega)|$ gets its maximum with the value of 1. We suppose that $\mathbf{\Omega}(R)$ is being used to denote the set of all normal windows.

Definition 2.2 For a time series $f(t)$, its NTFT $\mathbf{\Psi}$ is defined as

$$\mathbf{\Psi} f(\tau, \varpi) = \int_R f(t)\psi^*(t-\tau, \varpi)\mathrm{d}t, \quad \tau, \varpi \in R \tag{2}$$

where τ is the time index, ϖ is the frequency index, '*' denotes the complex conjugation operator, and transform kernel $\psi(t, \varpi)$ satisfies

$$\hat{\psi}(\omega, \varpi) = \left|\hat{\psi}(\omega, \varpi)\right| = \textbf{Maximum} = 1 \Leftrightarrow \omega = \varpi \tag{3}$$

in which $\hat{\psi}(\omega, \varpi) = F[\psi(t, \varpi)]_\omega$ and $\hat{\psi}(\omega, \varpi)$ is function of ω and ϖ. The meaning of relation (3) is similar to relation (1).

A typical NTFT kernel can be constructed as

$$\psi(t, \varpi) = |\mu(\varpi)|\, w(\mu(\varpi)t)\exp(i\varpi t),\ w(t) \in \mathbf{\Omega}(R),\ (\mu(\varpi) \in R) \dot{\neq} 0 \tag{4}$$

where dot means "almost anywhere". The rescaling index $\mu(\varpi)$ can be almost anything other than zero, for instance, ϖ, $\varpi^{2/3}$, ϖ^5 and so on. Letting $\mu(\varpi) = 1$ in Eq. (4) yields a phase-updated GT and letting $\mu(\varpi) = \varpi$ in Eq. (4) yields a normal wavelet transform. In this study, the latter is used for the time–frequency analysis and for the long-term polar motion prediction.

For a multi-component signal $f(t)$ that consists of n sub-signals $h_1(t)$, $h_2(t)$, …, $h_n(t)$ with frequencies of $\varpi_1, \varpi_2, \ldots, \varpi_n$, respectively,

$$\begin{aligned} f(t) = h_1(t)+h_2(t)+\cdots+h_n(t) &= A_1\exp(i\varpi_1 t) \\ &+A_2\exp(i\varpi_2 t)+\cdots+A_n\exp(i\varpi_n t) \end{aligned} \tag{5}$$

where $A_1, A_2, \ldots, A_n$ are complex, its NTFT is

$$\begin{aligned} \mathbf{\Psi} f(\tau, \varpi) = h_1(\tau)\hat{w}\left(\frac{\varpi-\varpi_1}{\mu(\varpi)}\right)+h_2(\tau)\hat{w}\left(\frac{\varpi-\varpi_2}{\mu(\varpi)}\right) \\ +\cdots+h_n(\tau)\hat{w}\left(\frac{\varpi-\varpi_n}{\mu(\varpi)}\right) \end{aligned} \tag{6}$$

We fix the parameter τ_k as the current observation time. Letting $\tau = \tau_k$ and $\varpi = \varpi_1, \varpi_2, \ldots, \varpi_n$, respectively, one has

$$\begin{cases} \mathbf{\Psi} f(\tau_k, \varpi_1) = h_1(\tau_k)+h_2(\tau_k)\hat{w}\left(\frac{\varpi_1-\varpi_2}{\mu(\varpi_1)}\right)+\cdots+h_n(\tau_k)\hat{w}\left(\frac{\varpi_1-\varpi_n}{\mu(\varpi_1)}\right) \\ \mathbf{\Psi} f(\tau_k, \varpi_2) = h_1(\tau_k)\hat{w}\left(\frac{\varpi_2-\varpi_1}{\mu(\varpi_2)}\right)+h_2(\tau_k)+\cdots+h_n(\tau_k)\hat{w}\left(\frac{\varpi_2-\varpi_n}{\mu(\varpi_2)}\right) \\ \cdots \\ \mathbf{\Psi} f(\tau_k, \varpi_n) = h_1(\tau_k)\hat{w}\left(\frac{\varpi_n-\varpi_1}{\mu(\varpi_n)}\right)+h_2(\tau_k)\hat{w}\left(\frac{\varpi_n-\varpi_2}{\mu(\varpi_n)}\right)+\cdots+h_n(\tau_k) \end{cases} \tag{7}$$

Equation groups (7) can be rewritten as

$$\mathbf{T} = \mathbf{W}\mathbf{E} \tag{8}$$

where

$$\mathbf{T} = \begin{bmatrix} \mathbf{\Psi} f(\tau_k, \varpi_1) \\ \mathbf{\Psi} f(\tau_k, \varpi_2) \\ \vdots \\ \mathbf{\Psi} f(\tau_k, \varpi_n) \end{bmatrix},$$

$$\mathbf{W} = \begin{bmatrix} 1 & \hat{w}\left(\frac{\varpi_1-\varpi_2}{\mu(\varpi_1)}\right) & \cdots & \hat{w}\left(\frac{\varpi_1-\varpi_n}{\mu(\varpi_1)}\right) \\ \hat{w}\left(\frac{\varpi_2-\varpi_1}{\mu(\varpi_2)}\right) & 1 & \cdots & \hat{w}\left(\frac{\varpi_2-\varpi_n}{\mu(\varpi_2)}\right) \\ \vdots & \vdots & \vdots & \vdots \\ \hat{w}\left(\frac{\varpi_n-\varpi_1}{\mu(\varpi_n)}\right) & \hat{w}\left(\frac{\varpi_n-\varpi_2}{\mu(\varpi_n)}\right) & \cdots & 1 \end{bmatrix}, \quad \text{and}$$

$$\mathbf{E} = \begin{bmatrix} h_1(\tau_k) \\ h_2(\tau_k) \\ \vdots \\ h_n(\tau_k) \end{bmatrix} \tag{9}$$

Vector T represents NTFT coefficients, matrix W represents the frequency resolution (Liu and Hsu 2009) or harmonic amplitude weight (Liu and Hsu 2012), and vector E denotes the sub-signals at τ_k. The matrix W comes from the normal window and is independent of sub-signals, providing the basis for sub-signal component separation.

Note that the width of the normal window must not be extremely narrow to ensure the matrix W invertible. The detailed width depends on the distance between $\varpi_1, \varpi_2, \ldots, \varpi_n$. Then, sub-signals at τ_k can be obtained as

$$\mathbf{E} = \mathbf{W}^{-1}\mathbf{T} \tag{10}$$

where the $\mathbf{W}^{-1}$ means the inverse matrix of the matrix W.

Thus, the signal $f(t)$ can be extrapolated by

$$f(\tau_k + M) = \mathbf{E} \begin{bmatrix} \exp(i\varpi_1 M) \\ \exp(i\varpi_2 M) \\ \vdots \\ \exp(i\varpi_n M) \end{bmatrix} \tag{11}$$

where M is the extrapolation step, i.e., lead time. We use the instantaneous frequency, amplitude and phase at the current observation time τ_k to extrapolate the signal. So the current instantaneous information is important for prediction.

In practice, the signals are usually quasi-harmonic. If the frequency, amplitude and phase of the quasi-harmonic signal vary slowly, the prediction method mentioned above is also suitable.

3 Time–frequency analysis of the polar motion

3.1 Data source and preparation

In this study, the polar motion (PMx and PMy) time series covering the period from January 1, 1962 to December 31, 2012 is downloaded from the website of IERS Earth Orientation Center (ftp://hpiers.obspm.fr/iers/eop/eopc04-05). The sampling interval is 1 day. We constructed the complex polar motion series, which has a real part of PMx and an imaginary part of PMy.

We use the linear least squares adjustment to get the trend model of the polar motion. Thus, the detrended polar motion can be obtained by subtracting the trend model from the polar motion. The detrended polar motion is used to analyze the time–frequency characteristics of the polar motion.

3.2 Spectrum analysis of the polar motion

We obtained the normalized spectrum of the detrended polar motion using fast Fourier transform (FFT), as shown in Fig. 1.

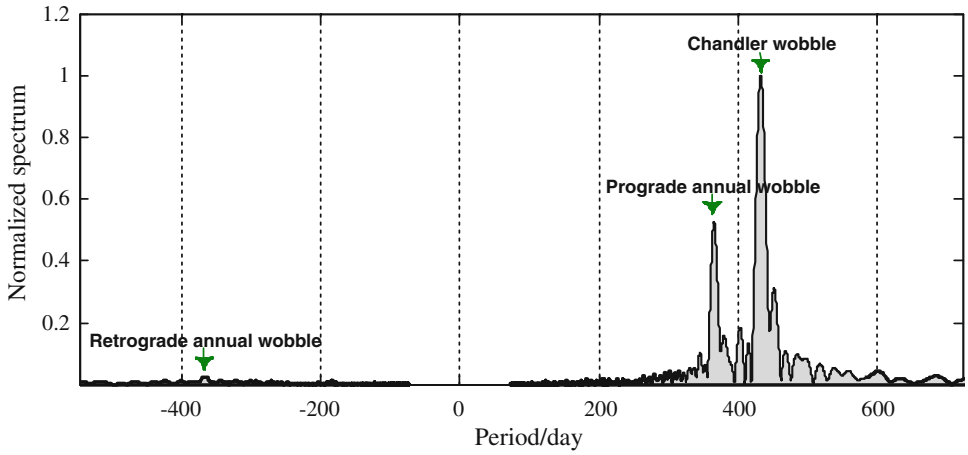

Fig. 1 Normalized spectrum of the detrended polar motion by FFT

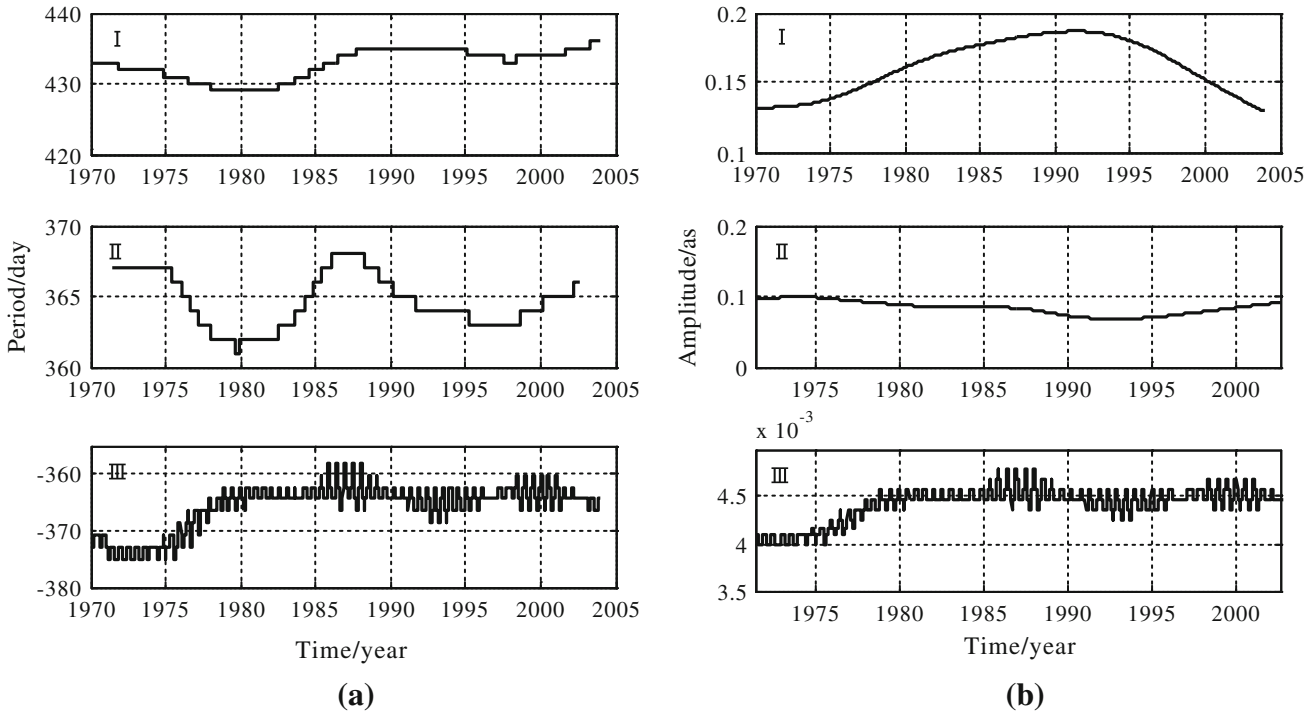

Fig. 2 The instantaneous frequency (**a**) and amplitude (**b**) of Chandler wobble (I), prograde (II) and retrograde (III) annual wobbles obtained via the normal wavelet transform

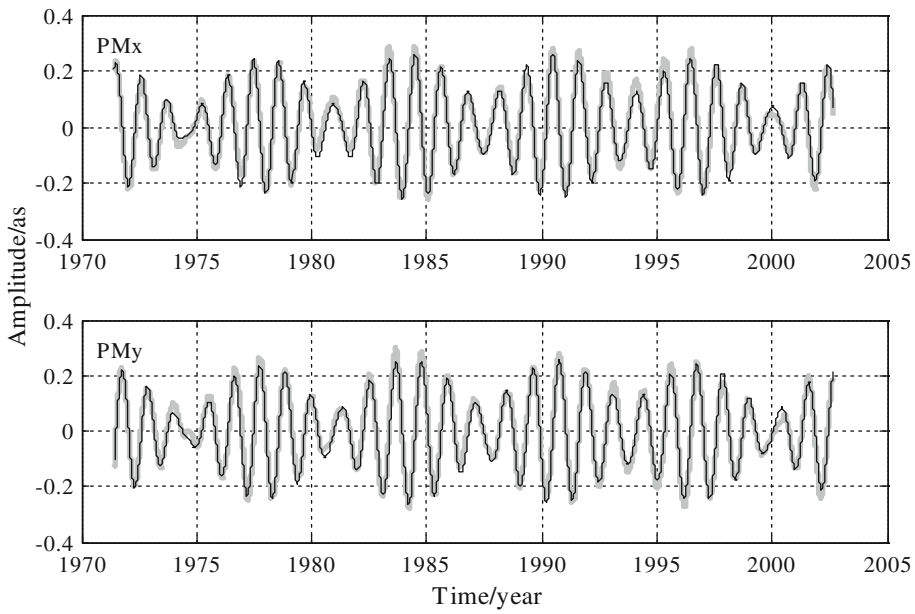

Fig. 3 The detrended polar motion (*the gray line*) and its corresponding fitting model (*the black line*)

Chandler wobble, prograde and retrograde annual components can be seen with periods of approximately 432, 365, and −366 days, respectively. Excitations to the latter two are almost identical. The response of the prograde annual wobble to the excitations is larger than the retrograde annual wobble, because the prograde annual wobble is rather closer in frequency to the Chandler wobble than the retrograde annual wobble.

The spectrum reflects only the averaged frequency. It cannot reflect the varying of frequency and amplitude with time. The instantaneous time–frequency parameters can be captured only through the time–frequency analysis.

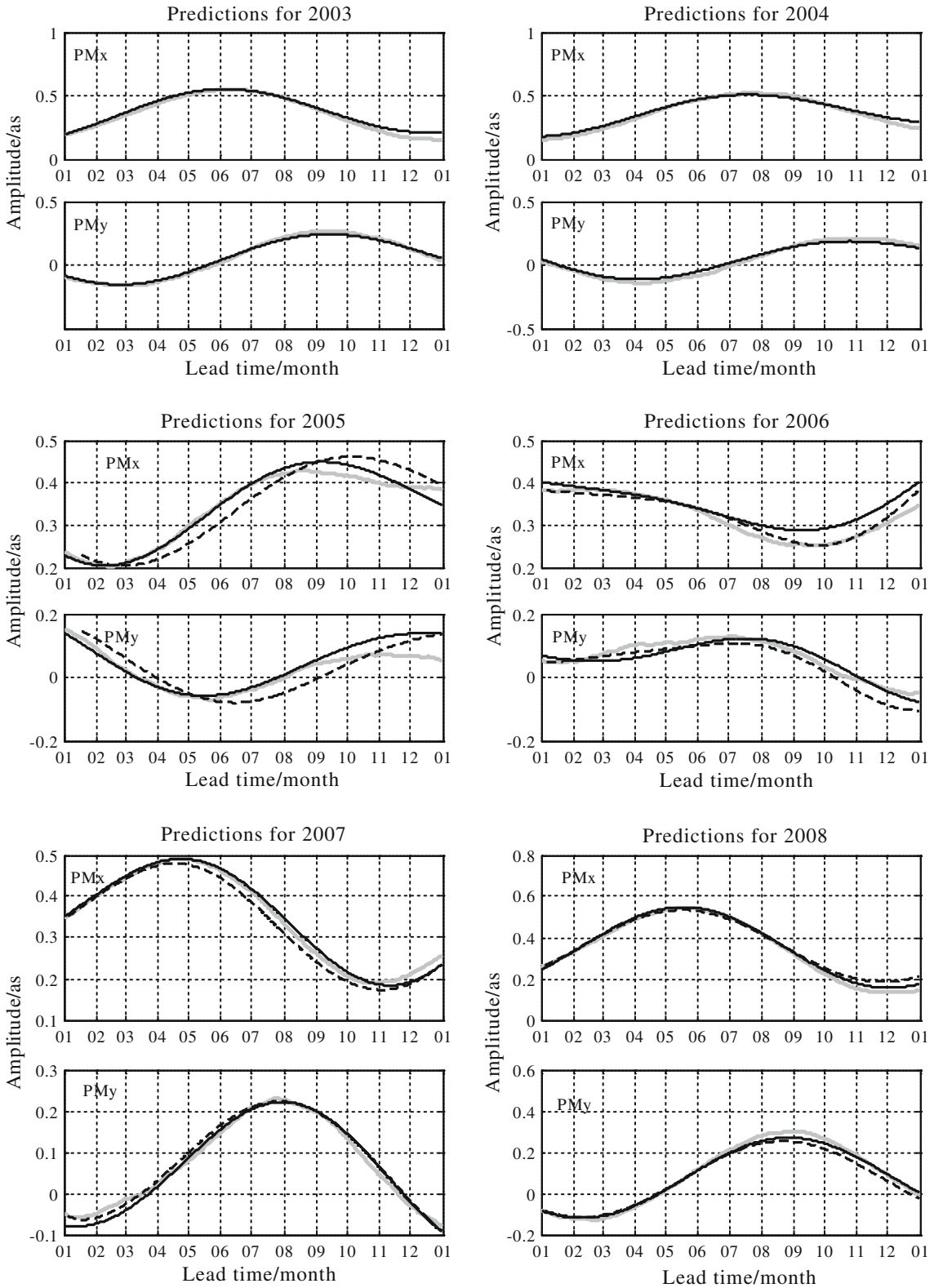

Fig. 4 The polar motion series (*the gray line*), the IERS "Bulletin A" predictions (*the black dash line*) and the NTFT predictions (*the black line*) from 2003 to 2012. The kernel function of NTFT is constructed as $\psi(t, \varpi) = |\varpi|\, w(\varpi t) \exp(i\varpi t)$, in which $w(t)$ is chosen as Eqs. (13) and (14) with $l = 12\pi$ days or higher.

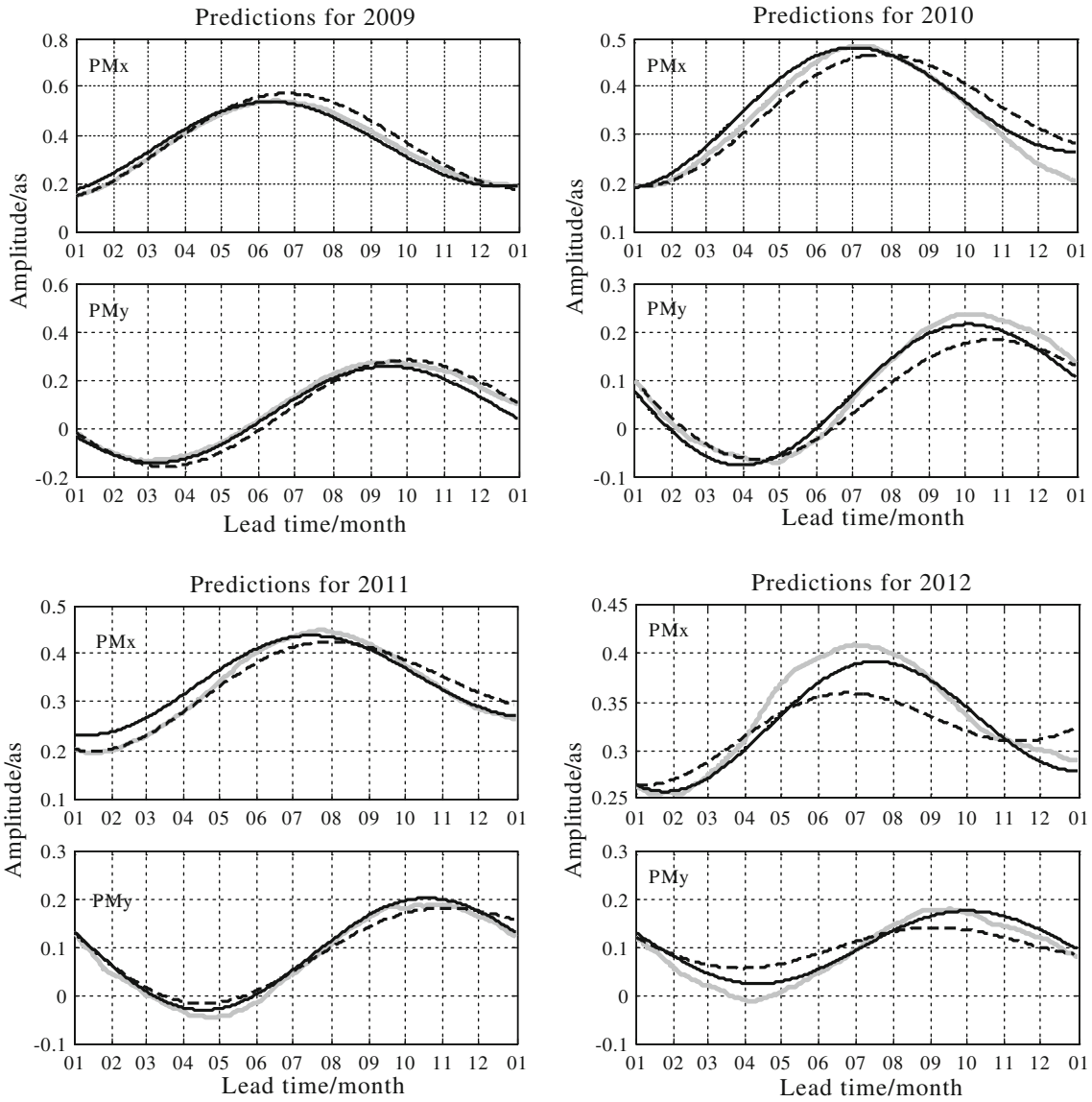

Fig. 4 continued

3.3 Time–frequency analysis of the polar motion

The normal wavelet transform is used to analyze the detrended polar motion. Its kernel function is constructed as $\psi(t, \varpi) = |\varpi|\, w(\varpi t) \exp(i\varpi t)$ and $w(t)$ is the normal Hamming window, i.e.,

$$w(t) = (1.08l)^{-1} \begin{cases} 0.54 + 0.46\cos(\pi t/l) & |t| \le l \\ 0 & \text{otherwise} \end{cases} \tag{12}$$

In order to separate the three wobbles, $l = 100$ according to the time–frequency resolution (Liu and Hsu 2009). The unit of t is day.

There are three maximum ridges along the time–frequency direction in the normal wavelet transform spectrum. The normal wavelet transform coefficients along the three ridges are nearly the three wobbles, respectively. Then we can extract the three wobbles at different times. The instantaneous frequency and amplitude of the three wobbles are computed and are shown in Fig. 2. We can also get fitting model of the detrended polar motion by adding the three main wobbles together, as shown in Fig. 3. Only the wobbles without edge effect are shown in Figs. 2 and 3.

It can be seen from Fig. 2 that the frequency and amplitude of the Chandler wobble, prograde and retrograde annual wobbles of the polar motion are slowly varying with time. So they can be considered as quasi-harmonic processes. Thus, instan-

taneous frequency and amplitude are necessary to depict the time–frequency characteristics of these wobbles. These factors are also the basis for the normal wavelet transform to predict the long-term polar motion.

The correlation between actual and fitting values is 0.9896 and 0.9907 for the PMx and for the PMy, respectively. The Root-mean-square error (RMSE) between them is 19.73 and 21.4 mas for the PMx and for the PMy, respectively. Both correlation coefficient and RMSE indicate the feasibility of the normal wavelet transform for long-term polar motion prediction.

4 Prediction of the polar motion

The detrended polar motion is quasi-harmonic. Therefore, the instantaneous time–frequency information of the polar motion at the current time should be the most useful for predicting its future. However, a natural problem in time–frequency analysis methods is edge effect. The edge effect makes the time–frequency analysis results at the current time implausible.

In order to obtain the accurate time–frequency information at the current time, we use the normal half-window to construct the kernel function. In the rest of this paper, numerical examples use the normal half-Hamming window, i.e., if $\varpi \geq 0$,

$$w(t) = 2(1.08l)^{-1} \begin{cases} (0.54 + 0.46\cos(\pi t/l)) & -l \leq t \leq 0 \\ 0 & \text{otherwise} \end{cases} \tag{13}$$

and if $\varpi \leq 0$

$$w(t) = 2(1.08l)^{-1} \begin{cases} (0.54 + 0.46\cos(\pi t/l)) & 0 \leq t \leq l \\ 0 & \text{otherwise} \end{cases} \tag{14}$$

In Eqs. (13) and (14), $l(>0)$ denotes the original width of the window. The unit of t is day. We can get the instantaneous frequency, amplitude and phase at the current time using only the history data. It is the accurate instantaneous information at the current time, especially the phase information, that makes the NTFT particularly suitable for the long-term prediction.

The detailed steps are as follows: (1) The detrended polar motion is calculated by subtracting the linear trend from the polar motion series; (2) The instantaneous frequencies of sub-signals at the current time are determined through its normal wavelet transform spectrum; (3) Take the instantaneous frequencies into Eq. (7), then we can get the instantaneous time–frequency information at current time by Eq. (10); and (4) Extrapolate the polar motion series according to Eq. (11).

Table 1 Correlation coefficient between the polar motion series and predictions

Prediction year	IERS "Bulletin A"		NTFT	
	PMx	PMy	PMx	PMy
2003	–	–	0.9967	0.9985
2004	–	–	0.9974	0.9969
2005	0.9769	0.9329	0.9940	0.9344
2006	0.9769	0.9833	0.9494	0.9420
2007	0.9978	0.9948	0.9964	0.9933
2008	0.9974	0.9971	0.9987	0.9992
2009	0.9944	0.9912	0.9886	0.9971
2010	0.9305	0.9907	0.9906	0.9894
2011	0.9767	0.9885	0.9877	0.9985
2012	0.9668	0.9737	0.9767	0.9812
Mean value	0.9772	0.9815	0.9876	0.9830

Table 2 RMSE (mas) of the predictions

Prediction year	IERS "Bulletin A"		NTFT	
	PMx	PMy	PMx	PMy
2003	–	–	21.97	13.51
2004	–	–	19.56	21.91
2005	24.84	30.40	14.00	29.10
2006	11.65	25.36	28.06	19.20
2007	16.73	11.94	10.27	14.04
2008	26.96	28.15	13.91	14.67
2009	25.25	27.14	19.38	22.45
2010	37.39	33.77	21.38	19.64
2011	18.75	17.75	21.47	19.63
2012	29.20	36.12	14.94	18.48
Mean value	23.85	26.33	18.49	19.26

Table 3 RMSE (mas) of the predictions by other methods

Lead time /days		PMx		PMy	
		180	360	180	360
Kosek et al. (2007)	LS	60.4	45.8	61.4	46.8
	LS+AR (AIC)	23.5	33.1	26.9	34
	LS+AR (emp)	23.8	29.5	25.3	30.6
Akyilmaz et al. (2011)	Fuzzy-wavelet	32.82	39.79	35.60	38.51
	FIS	29.123	34.983	31.612	31.252
Liao et al. (2012)	ANN	32.82	39.79	35.60	38.51
This paper	NTFT	16.52	18.49	17.71	19.26

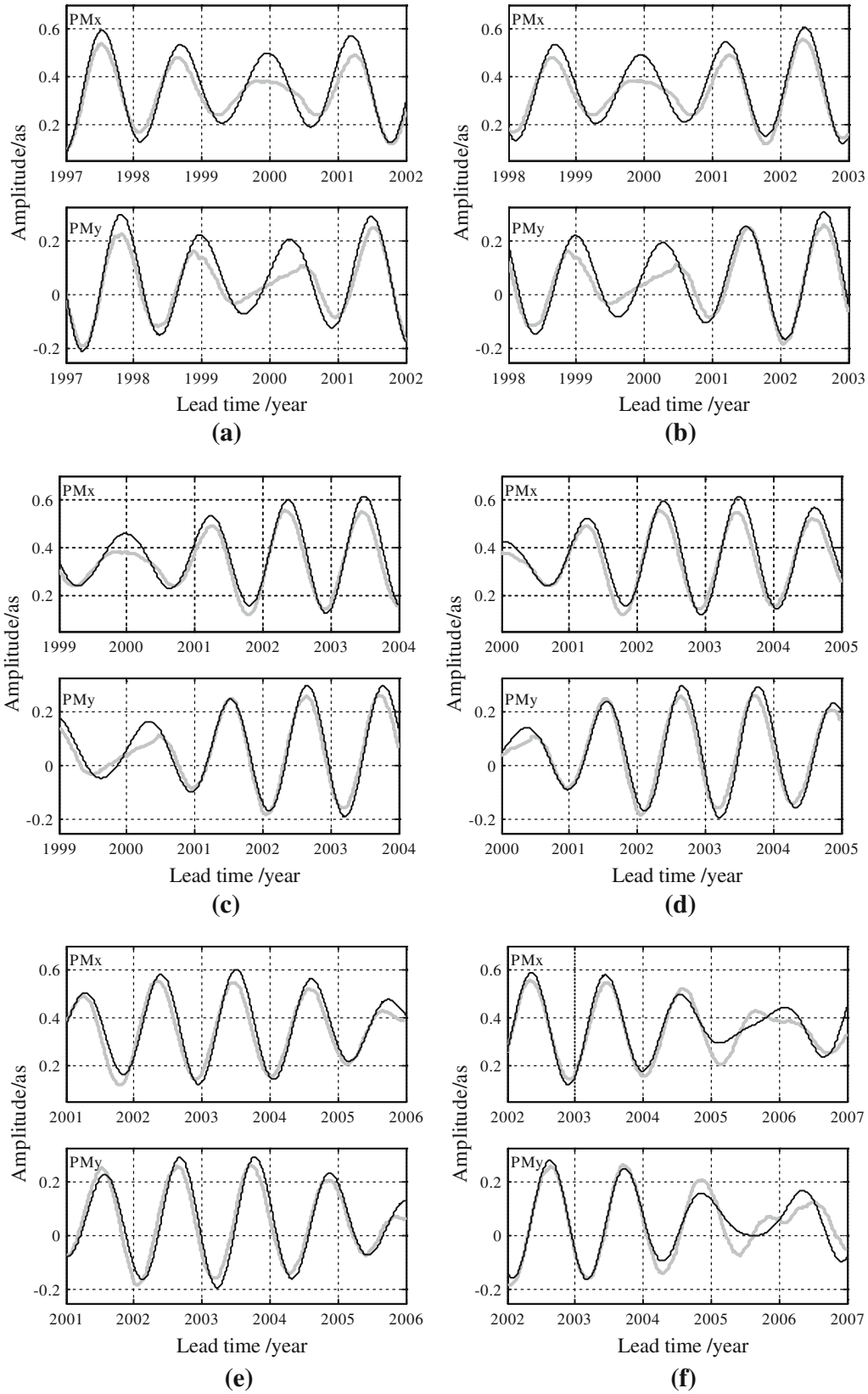

Fig. 5 The polar motion series (*the gray line*) and the NTFT predictions (*the black line*) from 1997. The kernel function of NTFT is constructed as $\psi(t, \varpi) = |\varpi|\, w(\varpi t) \exp(i\varpi t)$, in which $w(t)$ is chosen as Eqs. (13) and (14) with $l = 20\pi$ days or higher

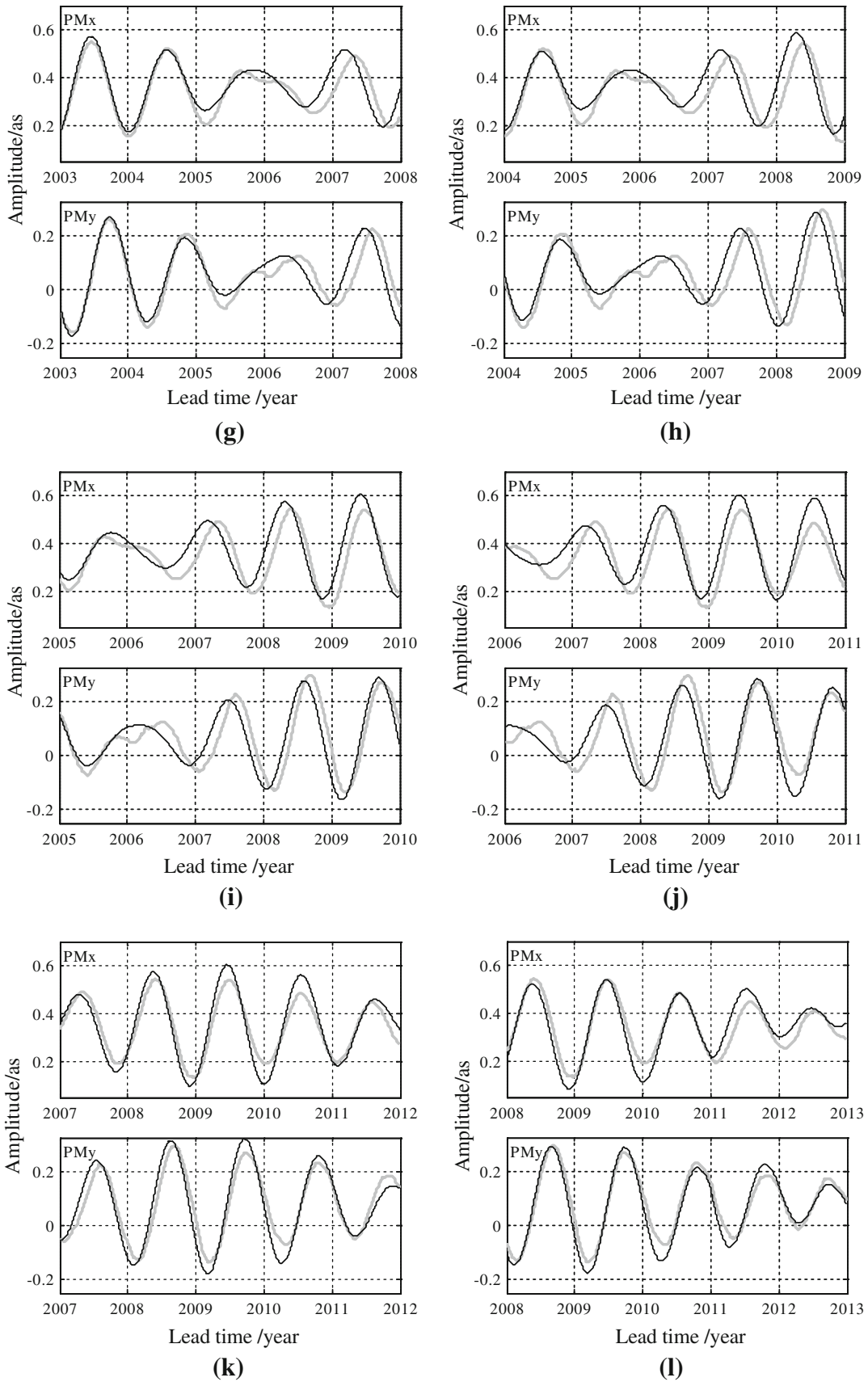

Fig. 5 continued

Table 4 Correlation coefficient and RMSE (mas) of 5-year-lead predictions

Current observation time	Correlation coefficient		RMSE/mas	
	PMx	PMy	PMx	PMy
Dec. 31, 1996	0.9648	0.9599	51.19	52.48
Dec. 31, 1997	0.9611	0.9428	48.30	48.86
Dec. 31, 1998	0.9756	0.9712	41.83	35.92
Dec. 31, 1999	0.9757	0.9728	40.80	34.67
Dec. 31, 2000	0.9655	0.9617	42.47	39.11
Dec. 31, 2001	0.9589	0.9474	35.86	38.92
Dec. 31, 2002	0.9200	0.9205	44.85	43.83
Dec. 31, 2003	0.8588	0.8463	59.63	59.21
Dec. 31, 2004	0.8553	0.8746	65.06	56.83
Dec. 31, 2005	0.8829	0.8986	65.35	56.18
Dec. 31, 2006	0.9632	0.9554	45.30	44.05
Dec. 31, 2007	0.9569	0.9739	35.39	31.93
Mean value	0.9366	0.9354	48.00	45.17

4.1 One-year-lead prediction

One-year-lead predictions from 2003 to 2012 are obtained with the steps described above. The results are compared with the IERS "Bulletin A" predictions that have the comparable lead time. The prediction accuracies are measured by the correlation coefficient and RMSE as well. The results are shown in Fig. 4 and the statistical results are listed in Tables 1 and 2.

Table 1 shows that the correlations in the predictions of 2006 are particularly smaller compared with others in the NTFT method. This result is caused by the abnormality during the second half of 2005 and first half of 2006, as indicated in the Sect. 4.2. The statistical results of 10 predictions show that the observations and predictions are highly correlated with the average degree of more than 0.98 for both PMx and PMy.

The mean RMSE of PMx and PMy is 18.49 and 19.26 mas in the NTFT method, respectively, which is less than that of IERS "Bulletin A". This mean value is significantly less than that of other methods listed in Table 3. Furthermore, the RMSE of other methods (Table 3) increases with lead time, while the RMSE of the NTFT method changes a little (not more than 2 mas) with the lead time.

4.2 Five-year-lead prediction

Our method can also be used for considerably longer-term prediction. From 1997, 5-year-lead predictions are made. The results are shown in Fig. 5. Correlation coefficient and RMSE are also used to assess prediction accuracy. Both are listed in Table 4.

An abnormality during the second half of 2005 and first half of 2006 can be seen in Fig. 5. The abnormality causes a phase delay of approximately 40 days. This delay is significant in predictions for 2007, 2008, and 2009 as shown in Fig. 5g–j. In Fig. 5k–l, the predictions starting from 2007 and 2008 return to the normal state. It indicates that the non-stationary behavior of the polar motion process

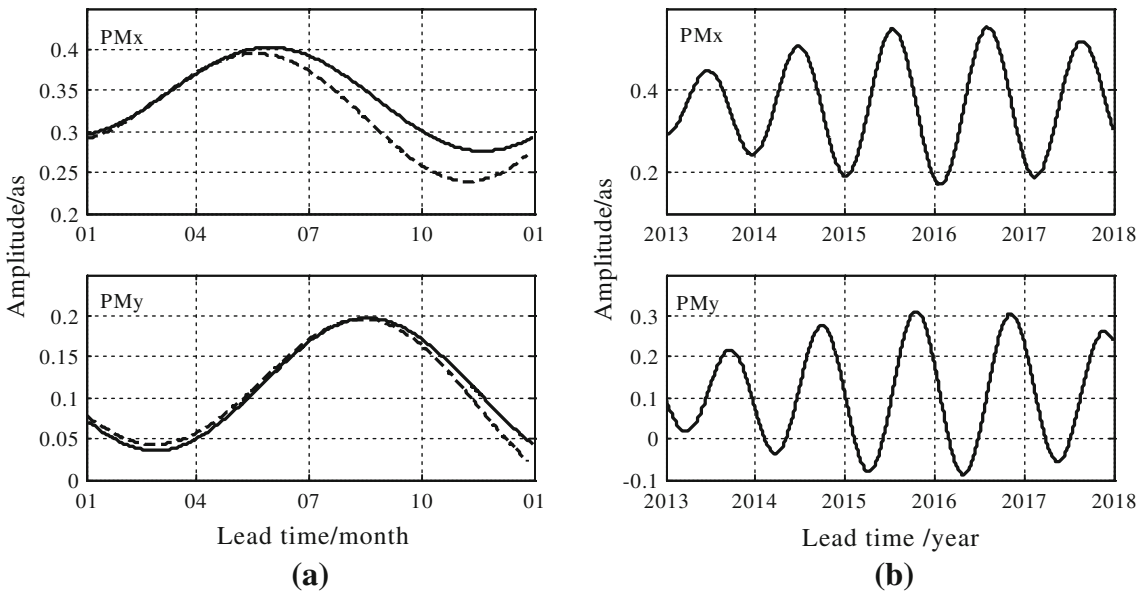

Fig. 6 The 1-year-lead predictions obtained through IERS "Bulletin A" (*the dash line*) and NTFT method (*the black line*) for 2013 (**a**) and 5-year-lead predictions from 2013 to 2017 (**b**) by NTFT.

during 2005–2006 causes the poor 5-year-lead predictions from 2003 to 2008, 2004 to 2009, 2005 to 2010 and 2006 to 2011.

The observations and 5-year-lead predictions are highly correlated with the correlation coefficient larger than 0.93 for both PMx and PMy. The average RMSEs for the PMx and the PMy are 48.00 and 45.17 mas, respectively.

4.3 Predictions after 2013

The 1-year-lead predictions for 2013 and 5-year-lead predictions from 2013 to 2017 are reported in Fig. 6. Parameters associated with the algorithm are selected as shown in previous figures. The predictions can be used to verify the effectiveness of the algorithm.

5 Conclusion

In this paper, we explain how the NTFT can be used for time–frequency analysis and long-term prediction. The Chandler wobble, prograde and retrograde annual wobbles of the polar motion can be considered as quasi-harmonic processes, as indicated by the NTFT. Based on these factors, a prediction method based on the NTFT is proposed. The NTFT with a half-window captures the instantaneous frequency, amplitude and phase accurately at the current time. It enables our method particularly suitable for long-term prediction.

In the numerical examples, the mean correlation between the observations and 1-year-lead predictions are higher than 0.98, and the correlation is higher than 0.93 in the case of the 5-year-lead prediction. The mean RMSE of the 1-year-lead prediction is less than that of other methods listed in Table 3. The comparison between the IERS "Bulletin A" and the NTFT predictions shows that our approach performs better in 1-year-lead prediction. Furthermore, the 5-year-lead predictions also can be made.

The difficult period for the 5-year-lead predictions is the second half of 2005 and first half of 2006. There is an abnormal phase delay of approximately 40 days. Finally, 1-year-lead predictions for 2013 and 5-year-lead predictions from 2013 to 2017 are provided.

Acknowledgments We are grateful to the International Earth Rotation and Reference Systems Service (IERS) for providing the polar motion data. This research is supported by NSFC 41074050 and by 2011YQ120045 of Ministry of Science and Technology of the People's Republic of China.

References

Kalarus M, Schuh H, Kosek W, Akyilmaz O (2010) Achievements of the Earth orientation parameters prediction comparison campaign. J Geod 84:587–596

Xu XQ, Zhou YH, Liao XH (2012) Short-term Earth orientation parameters predictions by combination of the least-squares, AR model and Kalman filter. J Geodyn 62:83–86

Petrov S, Brzeziński A, Gubanov V (1995) A stochastic model for polar motion with application to smoothing, prediction and combining. Artif Satell 31:51–70

Kosek W, McCharty DD, Luzum BJ (1998) Possible improvement of Earth orientation forecast using autocovariance prediction procedures. J Geod 72(4):189–199

Kosek W (2002) Autocovariance prediction of complex-valued polar motion time series. Adv Space Res 30(2):375–380

Schuh H, Ulrich M, Egger D, Müller J, Schwegmann W (2002) Prediction of Earth orientation parameters by artificial neural networks. J Geod 76:247–258

Akulenko LD, Kumakshev SA, Markov YG (2002) Motion of the Earth's pole. Dokl Phys 47:78–84

Xu XQ, Zotov L, Zhou YH (2012) Combined Prediction of Earth orientation parameters. China Satellite Navigation Conference (CSNC) 2012 Proceedings. Lect Notes Electr Eng 160:361–369

Akyilmaz O, Kutterer H (2004) Prediction of Earth rotation parameters by fuzzy inference systems. J Geod 78(1—-2):82–93

Akyilmaz O, Kutterer H, Shum CK, Ayan T (2011) Fuzzy-wavelet based prediction of Earth rotation parameters. Appl Soft Comput 11:837–841

Kosek W, Kalarus M, Niedzielski T (2007) Forecasting of the Earth orientation parameters comparison of different algorithms. In: Capitaine N (ed) Proceedings of the "Journèes systèmes de deréférence spatio-temporels (2007) Observatoire de Paris, 17–19 Sept 2007, Paris, France. ISBN 978-2-901057-59-8, pp 155–158

Liao DC, Wang QJ, Zhou YH, Liao XH, Huang CL (2012) Long-term prediction of the Earth orientation parameters by the artificial neural network technique. J Geodyn 62:87–92

Zhu SY (1982) Prediction of polar motion. Bull Géodésique 56:258–273

Liu LT, Hsu H (2009) Time–frequency transform: inversion and normalization. Hubei Science and Technology Press, Hubei

Liu LT, Hsu H (2012) Inversion and normalization of time-frequency transform. Appl Math Inf Sci 6(1S):67–74